

A General Framework for Self-Supervised Denoising with Patch Aggregation

Huy Minh Nhat Nguyen

Department of Computer Science and Engineering
Vietnamese German University
Ho Chi Minh City, Vietnam
10423045@student.vgu.edu.vn

Chau Vinh Hoang Truong

Department of Computer Science and Engineering
Vietnamese German University
Ho Chi Minh City, Vietnam
16076@student.vgu.edu.vn

Triet Hoang Minh Dao

Department of Computer Science and Engineering
Vietnamese German University
Ho Chi Minh City, Vietnam
10423179@student.vgu.edu.vn

Cuong Tuan Nguyen

Department of Computer Science and Engineering
Vietnamese German University
Ho Chi Minh City, Vietnam
cuong.nt2@vgu.edu.vn

Abstract—Optical Coherence Tomography (OCT) is a widely used non-invasive imaging technique that provides detailed three-dimensional views of the retina, which are essential for the early and accurate diagnosis of ocular diseases. Consequently, OCT image analysis and processing have emerged as key research areas in biomedical imaging. However, acquiring paired datasets of clean and real-world noisy OCT images for supervised denoising models remains a formidable challenge due to intrinsic speckle noise and practical constraints in clinical imaging environments.

To address these issues, we propose SDPA++: A General Framework for Self-Supervised Denoising with Patch Aggregation. Our novel approach leverages only noisy OCT images by first generating pseudo-ground-truth images through self-fusion and self-supervised denoising. These refined images then serve as targets to train an ensemble of denoising models using a patch-based strategy that effectively enhances image clarity. Performance improvements are validated via metrics such as Contrast-to-Noise Ratio (CNR), Mean Square Ratio (MSR), Texture Preservation (TP), and Edge Preservation (EP) on the real-world dataset from the IEEE SPS Video and Image Processing Cup. Notably, the VIP Cup dataset contains only real-world noisy OCT images without clean references, highlighting our method's potential for improving image quality and diagnostic outcomes in clinical practice.

Index Terms—OCT, Image Denoising, Self-supervised Learning, Patch Ensemble.

I. INTRODUCTION

1) **Background:** Optical Coherence Tomography (OCT) is a pivotal imaging technology in ophthalmology, enabling detailed cross-sectional visualization of the retina. This technique is critical for diagnosing and managing conditions such as Age-related Macular Degeneration (AMD), Diabetic Retinopathy (DR), and Diabetic Macular Edema (DME). However, OCT images are frequently affected by speckle noise and other imaging artifacts, which complicate interpretation and may lead to inaccuracies in diagnosis.

2) **Dataset Description:** The Signal Processing Society's 2024 Video and Image Processing Cup (VIP Cup) [1] challenges participants to enhance OCT image quality using a

dataset composed of noisy OCT B-scan images. These scans are divided into three classes:

- Normal/healthy (42 subjects)
- Diabetic patients with DME (30 subjects)
- Non-diabetic patients with ocular diseases such as AMD, CNV, or Macular Hole (MH)

Each subject has between 30 to 300 grayscale B-scan images at 300×300 resolution. Combining images from all subjects yields about 18,000 noisy OCT scans for the denoising challenge. No clean “ground truth” scans are available, highlighting the need for self-supervised or unsupervised methods.

3) **Motivation:** Traditional denoising algorithms such as non-local means [2], wavelet-based techniques [3], and median filtering [4] have been applied to enhance OCT image quality. While computationally straightforward, these conventional approaches often struggle to remove heavy speckle noise while preserving fine anatomical structures. Further, supervised learning-based algorithms typically require paired noisy and clean images, which are difficult to obtain in medical settings.

To overcome this limitation, self-supervised and unsupervised strategies have garnered attention. Techniques like self-fusion [5], Blind-Spot networks [6], Noise2Noise [7], Noise2Void [8], and Noise2Self [9] aim to learn denoising directly from noisy data. However, simply applying blind-spot or neighbor-based methods to extremely noisy data can still yield suboptimal results, particularly if the noise level is high.

4) **Contribution:** We propose a novel two-stage pipeline that creates a pseudo-clean reference from noisy images alone, then uses multiple self-supervised and supervised denoising models to refine the results further. Our main contributions are: (i) **Self-fusion pre-processing:** We exploit the 3D volume nature of OCT data by fusing neighboring B-scans to remove noise. (ii) **Self-supervised refinement:** We apply a neighbor-based self-supervised method to generate pseudo-ground-truth

images without requiring any clean references. **(iii) Patch-ensemble of multiple models:** We train advanced denoising models (e.g., Restormer, NAFNet, CGNET and diffusion-based models) using pseudo-clean targets, then fuse their outputs via a patch-based ensemble to achieve superior denoising quality.

Figure 1 illustrates an overview of our self-supervised and ensemble-based denoising framework for OCT images.

II. RELATED WORKS

A. Traditional Denoising Methods

Conventional denoising techniques typically rely on mathematical/statistical modeling. Non-local means [2] identifies and averages similar patches across an image, effectively removing noise but sometimes blurring features if the patch similarity criteria are not carefully tuned. Wavelet thresholding [3] decomposes images into multiple scales/frequencies, selectively attenuating noise but risking loss of fine details when thresholding is severe. Median filtering [4] replaces each pixel’s intensity with the median in a local neighborhood, effectively removing outliers but often sacrificing edge sharpness. Although these methods are simple and interpretable, their performance can degrade significantly in OCT scans with heavy speckle noise or complex structures.

B. Supervised Denoising Methods

Supervised deep learning approaches rely on paired noisy-clean datasets. U-Net [11] introduced skip connections to preserve high-resolution spatial information in medical image segmentation, and by extension, denoising. Restormer [12] uses a transformer-based architecture that captures long-range dependencies, improving restoration quality. NAFNet [13] refines network design to handle a wide range of image restoration tasks with fewer parameters. CascadedGaze (CGNet) [17], an efficient encoder-decoder architecture with a novel Global Context Extractor that captures global information without self-attention. Though these methods are powerful, they presume the availability of clean reference images, which is often unrealistic in clinical OCT data acquisition.

C. Self-Supervised and Unsupervised Denoising Methods

In the absence of clean references, self-supervised paradigms remove the need for paired data. Blind-spot methods—Noise2Void [8] and Noise2Self [9]—mask input pixels and train the network to predict them from surrounding context, preventing identity shortcuts and forgoing ground truth. Noise2Noise [7] instead learns from paired noisy realizations of the same scene, while Neighbor2Neighbor [10] relaxes this further by pairing randomly subsampled patches within a single image volume.

Self-fusion [5] aggregates adjacent slices/frames to form a cleaner proxy. Blind2Unblind [14] and AP-BSN [15] refine blind-spot training and account for spatially correlated noise. Generative approaches based on Denoising Diffusion Probabilistic Models (DDPMs) [16] learn a reverse noising process, enabling flexible modeling of complex noise distributions for high-quality restoration.

III. METHODOLOGY

Our denoising framework consists of two main phases (see Fig. 1). In **Phase 1**, we generate pseudo-clean images from the original noisy dataset using two steps: self-fusion and self-supervised denoising. In **Phase 2**, these pseudo-clean outputs become the training targets for multiple denoising models, whose results are then combined via patch-based ensemble.

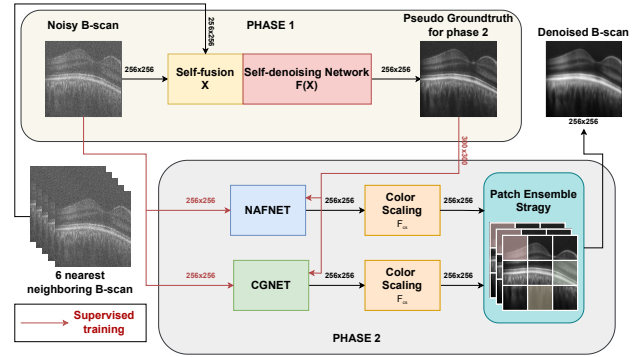


Fig. 1. Overview of proposed denoising method

A. Phase 1: Self-Fusion and Self-Supervised Refinement

a) Self-Fusion Preprocessing.: For each B-scan B_i in an OCT volume, we collect its six nearest neighboring B-scans B_{i-3}, \dots, B_{i+3} (excluding B_i itself). We register them to B_i if necessary (some volumes might be pre-aligned) and calculate a weighted fusion:

$$\tilde{B}_i(x, y) = \sum_{j=i-3}^{i+3} w_j(x, y) \cdot B_j(x, y),$$

where $w_j(x, y)$ is proportional to the patch similarity between B_j and B_i . This produces an intermediate self-fused image that reduces random speckle noise.

b) Neighbor2Neighbor.: Next, we apply the neighbor-based self-supervised training scheme proposed in [10] to refine \tilde{B}_i . By sampling random patches within \tilde{B}_i to form noisy pairs, the network learns to predict one patch from its neighbor, effectively denoising without requiring a clean ground truth. Let f_θ be our denoising network, and $(g_1(y), g_2(y))$ represent noisy patch pairs. The training loss:

$$\mathcal{L} = \|f_\theta(g_1(y)) - g_2(y)\|_2^2 + \gamma \cdot \mathcal{L}_{\text{reg}},$$

with a regularization \mathcal{L}_{reg} that penalizes disagreement between pairs of noisy predictions, promotes consistency. After training, $f_\theta(\tilde{B}_i)$ yields a pseudo-clean image C_i .

B. Phase 2: Supervised Denoising and Patch Ensemble

We then treat (B_i, C_i) as noisy-clean pairs to train two advanced models: NAFNet [13] and CGNET [17]. Each model learns to map $B_i \mapsto C_i$ under supervised settings. Although C_i is itself imperfect, it remains a far cleaner version than B_i , effectively serving as a stand-in for true ground truth.

Patch-Based Image Ensemble: Once these two models (NAFNET and CGNET) are trained, each produces a denoised

output for the same input B_i , each at a resolution of 256×256 . We aim to combine the strengths of each model via a sliding-window approach:

- 1) **Split into patches.** Split each model's 256×256 output into overlapping patches (window of size $k \times k$, with a stride that ensures slight overlap among consecutive patches).
- 2) **Local quality assessment.** At each patch location, evaluate a local measure of image quality using the combination of CNR, MSR, TP and EP metrics to gauge noise reduction and detail preservation.
- 3) **Select the best patch.** Among the three patches (one from each model) covering the same spatial region, select the patch that yields the highest score on the local quality metric.
- 4) **Blend via averaging.** In overlapping regions, average the selected patches' pixel values to create a seamless final image without boundaries or abrupt transitions.

This procedure ensures that the locally best denoising solution among the two networks is chosen, effectively reducing noise while preserving important details.

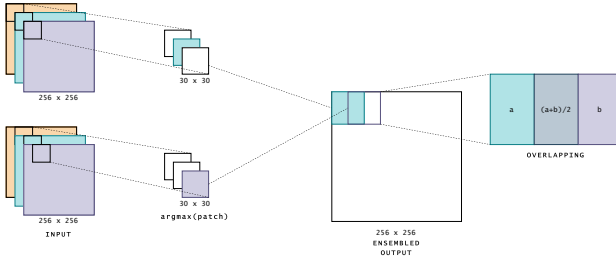


Fig. 2. Patch Ensemble Strategy

C. Color Scaling Post-Processing

After ensemble fusion, we apply an intensity rescaling step to maximize contrast:

$$I_{\text{norm}} = \frac{I}{255}, \quad F_{\text{cs}}(I_{\text{norm}}) = \left(\frac{I_{\text{norm}} - \min(I_{\text{norm}})}{\max(I_{\text{norm}}) - \min(I_{\text{norm}})} \right),$$

ensuring the darkest pixels map to 0 and the brightest map to 255 for improved visibility of retinal structures. More results in ablation study IV

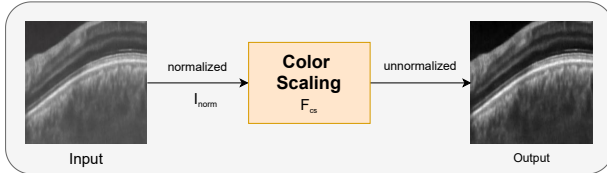


Fig. 3. The effect of applying the proposed contrast enhancement function on the image.

D. Model Inference

After completing Phase 1 and Phase 2 processing, the model produces a denoised OCT image. We then apply our method across the entire training dataset to obtain paired noisy and

denoised images. These paired samples are used to train a new CGNET model [17] using a supervised learning approach. Once trained, only the CGNET model is required for inference. See more in ablation study V

IV. EXPERIMENT

A. Dataset and metrics

In this paper, we only use the training set of the dataset provided in the Signal Processing Society's 2024 Video and Image Processing Cup challenge. The dataset has been captured in Didavarani clinic, Isfahan, Iran, using a custom-made Swept-Source OCT imaging system built in department of Biomedical Engineering, University of Basel. The central wavelength and spectral bandwidth of the OCT system are 1064 nm and 100 nm, respectively. The training set includes 100 OCT volume OCT data from 100 subjects, each volume belongs to one of three types (healthy, diabetic with DME, and non-diabetic patients with other ocular diseases), where each volume contains several B-scans of size 300x300. We split the training set into 2 smaller sets, training, and testing set with a ratio of 9:1. Besides that, we convert all images to a size of 256x256. For patch-based ensemble, we set the window size of 16x16 pixels, with a stride of 4 pixels.

For evaluation of the image quality as well as score calculation in ensemble strategy, we use 4 metrics Contrast-to-Noise Ratio (CNR), Mean-to-standard-deviation ratio (MSR), Texture Preservation (TP), and Edge Preservation (EP).

CNR: The Contrast-to-Noise Ratio (CNR) measures the contrast between significant structures and the background relative to noise, assessing how well the denoising algorithm enhances feature visibility while reducing noise. CNR is defined as:

$$CNR = 10 \log \left(\frac{|\mu_f - \mu_b|}{\sqrt{0.5(\sigma_f^2 + \sigma_b^2)}} \right)$$

where μ_f and σ_f represent the mean and standard deviation of the foreground regions, and μ_b and σ_b denote those of the background regions.

MSR: The Mean-to-Standard-Deviation Ratio (MSR) evaluates the clarity and sharpness of the image by comparing the signal's intensity to the noise variability, indicating the effectiveness of the noise reduction process. MSR is given by:

$$MSR = \frac{\mu_f}{\sigma_f}$$

where μ_f and σ_f are the mean and standard deviation of the foreground regions, respectively.

TP: Texture Preservation (TP) assesses the denoising algorithm's ability to retain the original texture of the image, which is crucial for accurate medical interpretation. TP is evaluated using the formula:

$$TP = \frac{\sigma_m^2}{(\sigma_m')^2} \sqrt{\frac{\mu_{\text{den}}}{\mu_{\text{in}}}}$$

where σ_m and σ_m' denote the standard deviation of the denoised and noisy images in the m-th Region of Interest (ROI),

respectively. μ_{den} and μ_{in} represent the mean values of the de-noised and noisy images, respectively.

EP: Edge Preservation (EP) measures how well the denoising algorithm preserves the edges of structures within the image, ensuring that critical boundaries are maintained for accurate medical analysis. EP is calculated as:

$$EP =$$

$$\frac{\Gamma(\Delta I'_m - \overline{\Delta I'_m}, \Delta I_m - \overline{\Delta I_m})}{\sqrt{\Gamma(\Delta I'_m - \overline{\Delta I'_m}, \Delta I'_m - \overline{\Delta I'_m})\Gamma(\Delta I_m - \overline{\Delta I_m}, \Delta I_m - \overline{\Delta I_m})}}$$

where I_m and I'_m are matrices that contain the de-noised and the noisy image regions, respectively, in the m-th ROI. Δ represents the Laplacian operator and Γ measures the correlation of images.

We validate SPDA++ on the VIP Cup dataset by splitting the 18,000 noisy B-scans into training and validation sets. Preliminary evaluations using metrics such as Contrast-to-Noise Ratio (CNR), Mean Square Ratio (MSR), Texture Preservation (TP), and Edge Preservation (EP) show that our two-stage strategy achieves notable improvements over direct blind-spot methods or single-model baselines.

B. Experimental Results

First, we evaluated the performance metrics of the proposed patch-based ensemble method (Patch Ensemble) as compared with Voting Ensemble, Self-fusion, and the single models of DDPM, NAFNET, and Restormer. From the result of Table I, Patch-based ensemble outperforms voting ensemble in MSR, TP, and EP, while slightly behind in CNR. From the result, we can see the instability in the performance of the single models, which complicates the global weighting in a voting ensemble approach. Consequently, this underscores the necessity to assess individual model outputs prior to their integration in the ensemble process.

TABLE I

COMPARISON OF VARIOUS METHODS ACROSS TWO FOLDS AND THEIR AVERAGE. THE BEST TOP 3 RESULTS ARE RED, BLUE AND BROWN.

	Fold 1				Fold 2				Average			
	CNR	MSR	TP	EP	CNR	MSR	TP	EP	CNR	MSR	TP	EP
Self-fusion	7.87	3.96	0.91	0.76	8.15	4.29	0.90	0.71	8.01	4.12	0.91	0.73
Neighbor2Neighbor	11.08	5.38	0.68	0.77	11.63	6.12	0.67	0.77	11.35	5.75	0.67	0.77
DDPM	11.89	3.47	1.01	0.73	12.68	4.10	0.97	0.74	12.28	3.79	0.99	0.73
NAFNET	11.49	3.38	1.21	0.73	12.90	4.25	1.13	0.73	12.19	3.81	1.17	0.73
Restormer	11.63	3.31	1.01	0.74	12.18	3.78	0.95	0.73	11.90	3.54	0.98	0.75
Voting Ensemble	11.99	3.24	1.10	0.73	13.00	3.93	1.04	0.73	12.49	3.58	1.07	0.73
Patch Ensemble	11.96	3.53	1.18	0.74	12.92	4.28	1.12	0.75	12.44	3.90	1.15	0.74

In the second experiment, we evaluated the performance of Patch Ensemble with different configurations of patch selection criteria. Table 2 shows the results of Patch Ensemble with the criteria based on single metrics of CNR, TP, MSR and EP as compared with the criteria using a weighted combination of multiple metrics (Patch Ensemble (All)). From the result, we can see that Patch Ensemble with the criteria using a single metric enhances the performance for that specific metric but reduces the performance of other metrics. We propose a combination of metrics as the selection criteria. The best combination of metrics is found experimentally: CNR*3 + MSR*2 + TP*5. With this approach, the ensemble method

achieves an effective trade-off among the evaluated metrics, thereby optimizing overall result quality.

TABLE II

COMPARISON OF VARIOUS PATCH ENSEMBLE SCORES ACROSS TWO FOLDS AND THEIR AVERAGE. THE BEST TOP 3 RESULTS ARE RED, BLUE, BROWN

	Fold 1				Fold 2				Average			
	CNR	MSR	TP	EP	CNR	MSR	TP	EP	CNR	MSR	TP	EP
Patch Ensemble (CNR)	12.09	3.55	1.10	0.74	13.12	4.25	1.07	0.75	12.60	3.90	1.09	0.74
Patch Ensemble (TP)	11.62	3.35	1.19	0.73	12.68	3.97	1.10	0.75	12.15	3.66	1.14	0.74
Patch Ensemble (MSR)	11.93	3.59	1.10	0.74	13.04	4.40	1.06	0.75	12.49	3.99	1.08	0.74
Patch Ensemble (EP)	11.62	3.44	1.01	0.74	12.44	4.00	0.95	0.76	12.03	3.72	0.98	0.75
Patch Ensemble (All)	11.96	3.53	1.18	0.74	12.92	4.28	1.12	0.75	12.44	3.90	1.15	0.74

Figure 4 shows the denoised images of a challenging input noise sample.

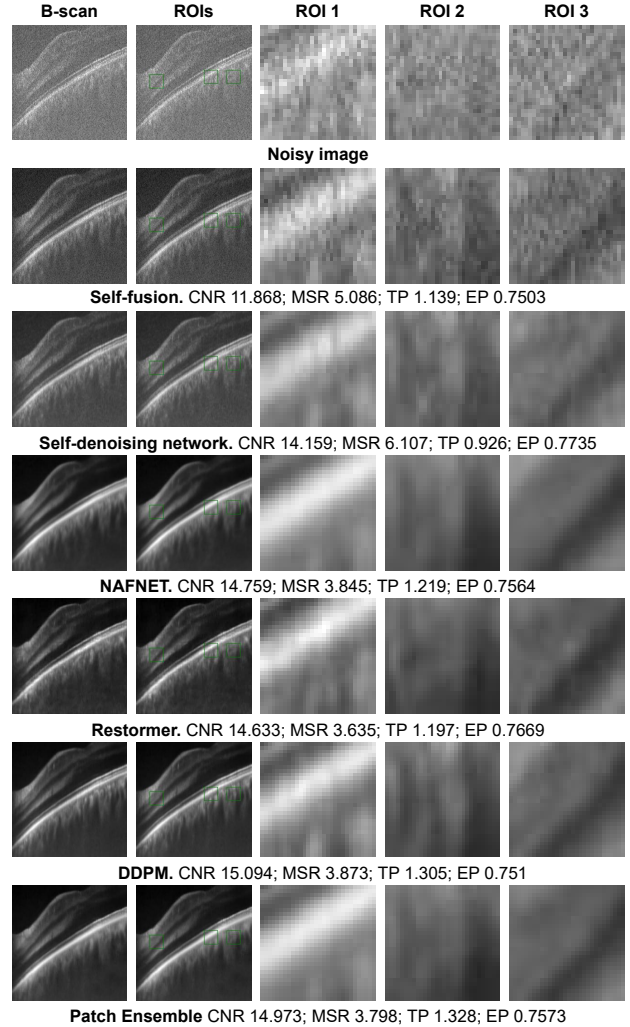


Fig. 4. Visual results of used methods on a B-scan

V. CONCLUSION

We introduced a novel two-phase denoising pipeline for OCT images, leveraging self-fusion, neighbor-based self-supervision, and a patch-based ensemble of advanced denoising networks. Our framework tackles the common challenge in medical image denoising: the unavailability of perfectly

clean ground truth data. By smartly creating pseudo-clean references and aggregating the strengths of multiple models, our method robustly suppresses speckle noise and preserves critical anatomical details. Experimental results on the noisy-only VIP Cup dataset demonstrate the effectiveness of our approach, paving the way for improved OCT image quality and more reliable clinical diagnoses.

REFERENCES

- [1] IEEE Signal Processing Society, “*IEEE Video and Image Processing Cup 2024: SS-OCT Image Analysis*,” [Online]. Available: <https://signalprocessingsociety.org/community-involvement/video-image-processing-cup> [Accessed: Apr. 11, 2025].
- [2] A. Buades, B. Coll, and J.-M. Morel, “A non-local algorithm for image denoising,” in *Proceedings of the 2005 IEEE Computer Society Conference on Computer Vision and Pattern Recognition (CVPR)*, vol. 2, pp. 60–65, 2005.
- [3] D. L. Donoho and I. M. Johnstone, “Ideal spatial adaptation via wavelet shrinkage,” *Biometrika*, vol. 81, no. 3, pp. 425–455, 1994.
- [4] T. S. Huang, G. J. Yang, and G. Y. Tang, “A fast two-dimensional median filtering algorithm,” *IEEE Transactions on Acoustics, Speech, and Signal Processing*, vol. 27, no. 1, pp. 13–18, 1979.
- [5] J. J. Rico-Jimenez, D. Hu, E. M. Tang, I. Oguz, and Y. K. Tao, “Real-time OCT image denoising using a self-fusion neural network,” *Biomedical Optics Express*, vol. 13, no. 3, pp. 1398–1409, 2022. doi:10.1364/BOE.451029
- [6] S. Laine, T. Karras, J. Lehtinen, and T. Aila, “High-quality self-supervised deep image denoising,” in *Advances in Neural Information Processing Systems 33 (NeurIPS 2019)*, pp. 6970–6980, 2019.
- [7] J. Lehtinen, J. Munkberg, J. Hasselgren, S. Laine, T. Karras, M. Aittala, and T. Aila, “Noise2Noise: Learning image restoration without clean data,” in *Proc. 35th Int. Conf. on Machine Learning (ICML)*, PMLR-80:2965–2974, 2018.
- [8] A. Krull, T.-O. Buchholz, and F. Jug, “Noise2Void – learning denoising from single noisy images,” in *Proc. IEEE/CVF Conf. on Computer Vision and Pattern Recognition (CVPR)*, pp. 2129–2137, 2019.
- [9] J. Batson and L. Royer, “Noise2Self: Blind denoising by self-supervision,” in *Proc. 36th Int. Conf. on Machine Learning (ICML)*, PMLR 97:524–533, 2019.
- [10] T. Huang, S. Li, X. Jia, H. Lu, and J. Liu, “Neighbor2Neighbor: Self-Supervised Denoising from Single Noisy Images,” in *Proceedings of the IEEE/CVF Conference on Computer Vision and Pattern Recognition (CVPR)*, pp. 14781–14790, 2021.
- [11] O. Ronneberger, P. Fischer, and T. Brox, “U-Net: Convolutional Networks for Biomedical Image Segmentation,” in *Proc. Medical Image Computing and Computer-Assisted Intervention (MICCAI)*, Lecture Notes in Computer Science, vol. 9351, pp. 234–241, 2015.
- [12] S. W. Zamir, A. Arora, S. Khan, M. Hayat, F. S. Khan, and M.-H. Yang, “Restormer: Efficient Transformer for High-Resolution Image Restoration,” in *Proc. IEEE/CVF Conference on Computer Vision and Pattern Recognition (CVPR)*, pp. 5728–5739, 2022.
- [13] L. Chen, X. Chu, X. Zhang, and J. Sun, “Simple Baselines for Image Restoration,” in *Computer Vision – ECCV 2022*, Lecture Notes in Computer Science, vol. 13667, pp. 17–33, 2022.
- [14] Z. Wang, J. Liu, G. Li, and H. Han, “Blind2Unblind: Self-Supervised Image Denoising with Visible Blind Spots,” in *Proc. IEEE/CVF Conf. on Computer Vision and Pattern Recognition (CVPR)*, 2022.
- [15] W. Lee, S. Son, and K. M. Lee, “AP-BSN: Self-Supervised Denoising for Real-World Images via Asymmetric PD and Blind-Spot Network,” in *Proc. IEEE/CVF Conf. on Computer Vision and Pattern Recognition (CVPR)*, 2022.
- [16] J. Ho, A. Jain, and P. Abbeel, “Denoising Diffusion Probabilistic Models,” in *Advances in Neural Information Processing Systems 33 (NeurIPS)*, 2020.
- [17] A. Ghasemabadi, M. K. Janjua, M. Salameh, C. Zhou, F. Sun, and D. Niu, “CascadedGaze: Efficiency in Global Context Extraction for Image Restoration,” *Transactions on Machine Learning Research (TMLR)*, 2024; arXiv:2401.15235.
- [18] B. Monroy, J. Bacca, and J. Tachella, “Generalized Recorrupted-to-Recorrupted: Self-Supervised Learning Beyond Gaussian Noise,” *arXiv preprint arXiv:2412.04648*, 2025. [Online]. Available: <https://arxiv.org/abs/2412.04648>

ABLATION STUDY

TABLE III
SELF-FUSION ADAPTATION DIFFERENCE

Method	Fold 1				Fold 2			
	CNR	MSR	TP	EP	CNR	MSR	TP	EP
Self-fusion	10.80	4.70	0.93	0.83	10.49	4.91	0.94	0.84
R2R [18]	8.231	4.55	0.98	0.78	7.65	4.60	0.97	0.78
Self-fusion + R2R	10.13	4.55	1.08	0.67	9.89	4.78	1.08	0.67
Neighbor2Neighbor	10.63	10.36	0.47	0.87	9.95	10.38	0.47	0.87
Self-fusion + Neighbor2Neighbor	13.46	5.90	0.73	0.84	13.20	6.28	0.74	0.84

TABLE IV
COLOR SCALING ADAPTATION DIFFERENCE

Method	Fold 1				Fold 2			
	CNR	MSR	TP	EP	CNR	MSR	TP	EP
Scaled CGNet	13.966	4.360	1.017	0.835	13.841	4.569	1.019	0.837
CGNet	13.946	5.220	0.726	0.844	13.822	5.748	0.700	0.845
Scaled NAFNET	14.542	3.776	1.159	0.822	14.573	4.277	1.103	0.832
NAFNET	14.531	6.177	0.728	0.844	14.561	6.973	0.721	0.847
Scaled Restormer	14.427	3.963	1.026	0.822	14.108	4.118	0.977	0.829
Restormer	14.452	7.494	0.539	0.847	14.134	7.710	0.523	0.849

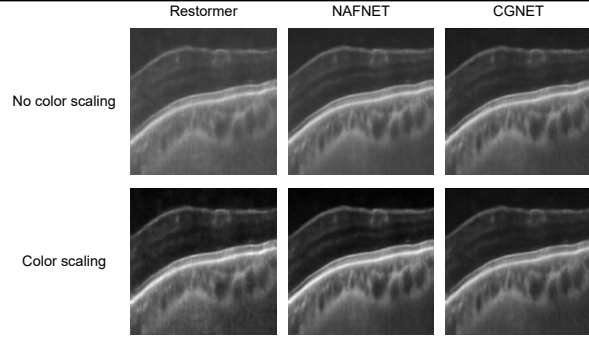


Fig. 5. Visual of color scaling method

TABLE V
PERFORMANCE COMPARISON OF DIFFERENT METHODS. THE BEST TOP 3 RESULTS ARE RED, BLUE, BROWN

Method	CNR	MSR	TP	EP
Scaled CGNET	13.966	4.360	1.017	0.835
Scaled NAFNET	14.542	3.776	1.159	0.822
Scaled Restormer	14.427	3.963	1.026	0.822
Patch Ensemble (CNR)	14.381	3.977	1.061	0.824
Patch Ensemble (MSR)	14.102	4.320	1.021	0.833
Patch Ensemble (TP)	13.463	3.728	1.180	0.822
Patch Ensemble (EP)	13.967	4.205	1.043	0.834
Patch Ensemble (cnr1-msr3-tp10)	13.930	4.183	1.130	0.828
Patch Ensemble (cnr3-msr2-tp5)	14.050	4.075	1.080	0.826
Patch Ensemble (cnr1-msr1-tp10)	13.777	4.021	1.149	0.825
Patch Ensemble (cnr3-tp5)	14.291	3.943	1.097	0.824
Patch Ensemble (cnr1-tp5)	14.111	3.867	1.1450	0.822
Patch Ensemble (cnr1-tp20)	13.868	3.758	1.178	0.822
Voting Ensemble	14.479	3.859	1.101	0.824
Model inference	14.601	3.832	1.221	0.819

Notation:

Patch Ensemble (cnr1-msr3-tp10) = CNR*1 + MSR*3 + TP*10.